第 35 卷第 5 期 2019 年 5 月
无 机 化 学 学 报 CHINESE JOURNAL OF INORGANIC CHEMISTRY
Vol.35 No.5 881-890

有机相化学镀铝法制备 Al/石墨烯复合材料粉末

段 政[1] 徐明英[1] 高建峰*,[1] 郝 敏[1] 刘 艳[1] 马 洁[1] 白培康[2]
([1]中北大学理学院,太原 030051)
([2]中北大学材料科学与工程学院,太原 030051)

摘要:采用有机相化学镀法制备了 Al/石墨烯复合材料粉末。使用傅里叶红外光谱仪、拉曼光谱仪、ASAP2020 全自动快速比表面与孔隙度分析仪和配备 EDS 能谱的扫描电子显微镜表征样品。结果表明,镀铝后,石墨烯表面的含氧基团基本消失,发生空间弯曲折叠形成包覆结构,导致中孔和大孔的形成,石墨烯层间距变大。此外,氮气吸附–脱附结果显示,Al/石墨烯复合材料粉末的孔道以微孔和中孔为主,Brunauer-Emmett-Teller 比表面积为 91 $m^2 \cdot g^{-1}$;通过 Barret-Joyner-Halenda 解吸模型计算得到的平均孔径为 8.77 nm,孔体积为 0.45 $cm^3 \cdot g^{-1}$。X 射线衍射分析并没有发现 Al_4C_3 晶体结构的出现,表明镀铝过程并未或生成很少(小于检测下限)脆相 Al_4C_3。最后,微观表面分析表明,当加入的 NaH 量略大于理论值时,实验结果与理想体系基本吻合,镀铝效果最佳。

关键词:有机相;化学镀;石墨烯;复合材料;粉末
中图分类号:TB333 **文献标识码**:A **文章编号**:1001-4861(2019)05-0881-10
DOI:10.11862/CJIC.2019.096

Synthesis of Al/graphene Composite Powder by Organic Phase Electroless Aluminum Plating

DUAN Zheng[1] XU Ming-Ying[1] GAO Jian-Feng*,[1] HAO Min[1] LIU Yan[1] MA Jie[1] BAI Pei-Kang[2]
([1]*School of Science, North University of China, Taiyuan* 030051, *China*)
([2]*School of Materials Science and Engineering, North University of China, Taiyuan* 030051, *China*)

Abstract: Al/graphene composite powder was prepared by an organic phase electroless aluminum plating method. The samples were characterized by Fourier transform infrared spectrometry, Raman spectrometry, ASAP2020 automatic specific surface area and porosity analyzer, and scanning electron microscope equipped with an energy dispersive-spectrometer (EDS). After electroless plating, the results showed that the oxygen-containing groups on the surface of graphene substantially decreased, and the cladding structure was formed by bending, which led to the formation of meso- and macropores; however, the spacing of the graphene layers was increased. In addition, the results of nitrogen adsorption showed that the pores of Al/graphene composite powder were dominated by micropores and mesopores, and the Brunauer-Emmett-Teller specific surface area was 91 $m^2 \cdot g^{-1}$; the average pore diameter and the pore volume calculated by the Barret-Joyner-Halenda desorption model was 8.77 nm and 0.45 $cm^3 \cdot g^{-1}$, respectively. The appearance of the crystal structure of Al_4C_3 was not found by X-ray diffraction analysis, indicating that the aluminum plating process did not produce or produce little (below the minimum limit of detection) brittle phase Al_4C_3. Finally, the microscopic surface analysis showed that when the amount of NaH added was slightly larger than the theoretical value, the experimental results were basically consistent with the ideal system, and the aluminum plating effect was the best.

Keywords: organic phase; electroless plating; graphene; composites; powder

收稿日期:2018-10-03。收修改稿日期:2019-03-13。
国家自然科学基金(No.51775521)资助项目。
*通信联系人。E-mail:jianfenggao@163.com

0 Introduction

In recent years, graphene has been a promising application prospect in the field of composite materials due to its excellent mechanical/functional properties and its unique physical/chemical properties[1-2]. Compared with graphene reinforced polymer matrix composites[1], graphene reinforced metal matrix composites (GNP-MMC), especially graphene reinforced aluminum matrix composites (Gr/Al), have not been studied in depth. The special atomic structure and properties of graphene make it an excellent additive for the preparation of reinforced and toughened composites. As distinct from other carbon allotropes such as carbon nanotubes (CNTs) and graphite, graphene has the characteristic 2D structure, which makes its specific surface area larger than those of CNTs or graphite[3], thus providing more area to interact with the matrix material. Therefore, graphene is an ideal reinforcement for the preparation of high-performance composites of any kind of matrix (whether polymer[4-6], ceramic[7-8], or metal[9-11]), and is expected to improve the mechanical and thermal properties of the aluminum matrix greatly when added to the aluminum matrix.

At present, the methods for preparing Gr/Al are casting[12-14], ball-milling[15-17], powder metallurgy[18] and friction stir processing (FSP)[19]. The nanosized (or microsized) Gr/Al can be prepared by casting and ball-milling methods; GNP-MMC prepared by powder metallurgy technology have good physical and chemical properties; Gr/Al prepared by the FSP method has few impurities. However, the above methods have a common problem that the complicated structure Gr/Al prepared by the above methods is longtime, high cost and even difficult to form the shape; moreover, the graphene is easily agglomerated in the matrix and has poor bonding property with the matrix interface. This cannot meet the material requirements of selective laser melting (SLM). The metal powder for SLM forming need high purity, good sphericity, small particle size and narrow particle size distribution (15 ~45 μm). Metal powder properties directly affect the stability of the SLM-forming process and the structural properties of the part. Because of the large difference in density between graphene and the aluminum matrix, poor wettability, and difficulty in uniform dispersion in the aluminum matrix, the preparation of Gr/Al powder has become a difficult problem in the application of SLM forming of additive manufacturing.

As far as we konw, there is no report on the synthesis of Al/graphene composites by the electroless plating method. The purpose of this study is to prepare the graphene/aluminum composite powder by uniformly plating metal aluminum atoms on the surface of graphene by the electroless plating method. Then, it can be used to prepare Gr/Al with metal aluminum or aluminum alloy, which is expected to solve the problem of easy agglomeration of graphene in the aluminum matrix, improve the interface between graphene and aluminum matrix, and meet the requirements of SLM for materials.

1 Experimental

1.1 Materials and reagents

The graphene/aluminum composite powder was prepared with aluminum powder (AR, purity 99.0%, purchased from Beijing Chemical Reagent Factory) and graphene (average layer 6 layers, Tangshan Jianhua Technology Development Co., Ltd.). Anhydrous aluminum chloride (purchased from Tianjin Chemical Reagent Factory) and iodine (purchased from Zhengzhou Chemical Reagent Factory) were sealed and stored in a brown bottle as an initiator. Furthermore, commercial NaH (purity 60%, purchased from Aladdin) was stored under a N_2 atmosphere to prevent oxygen/moisture exposure. Ethyl bromide (EtBr) (AR, purchased from Damao Chemical Reagent Factory) was distilled over anhydrous calcium chloride under N_2 atmosphere to remove water. Toluene and tetrahydrofuran (THF) (AR, purchased from Damao Chemical Reagent Factory) were distilled on sodium metal under N_2 atmosphere to remove water. H_2 (purity 99.99%, purchased from Taiyuan Industrial Gas Factory) as shielding gas was dried using a drying device.

1.2 Activation of aluminum powder

All reactions were carried out in an anhydrous

and anaerobic environment (hydrogen atmosphere). After repeated replacement with H_2, 3 g of aluminum powder, traces of anhydrous aluminum chloride and iodine (about 0.015 g), and 20 mL of freshly sealed ethidium bromide (EtBr) were added to a 250 mL three-necked flask. The mixture was heated to 39 ℃ and refluxed under a stream of hydrogen with stirring. After about 30 min, the reaction started, and the white smoke appeared, and then the mixture turned slightly black. As a result, the aluminum powder began to be activated and gradually generated an alkyl aluminum sesquihalide and activated aluminum. After 90 min, 15 mL of THF (as a complexing agent) was added to the reaction system, and the reaction was continued for 10 min. The mixture was quickly centrifuged, and the resulting supernatant (*i.e.*, alkyl aluminum sesquihalide) was sealed and stored.

1.3 Plating

All reactions were carried out in an anhydrous and anaerobic environment (hydrogen atmosphere). 0.2 g of graphene was weighed and added into 30 mL of toluene and the alkyl aluminum sesquihalide solution prepared in 1.2. The mixture was dispered uniformity by ultrasonic for 30 min, and 5.0 g of NaH was subsequently added, and the mixture was stirred and refluxed at 110 ℃ for 90 min. After the reaction was completed, the mixture was filtered, washed with absolute ethanol and distilled water successively, and then the filter residue was freeze-dried. Finally, the graphene/aluminum composite powder was obtained.

1.4 Characterization

Fourier transform infrared (FTIR) spectra of the samples (4 000~500 cm^{-1}) were measured on an FTIR-8400S infrared spectrometer using the KBr compression method. The microstructure and elemental composition of the samples were analyzed by the field emission scanning electron microscopy (SEM) (INSPECTF-50) (the acceleration voltage was 20 kV), energy dispersive spectroscopy (EDS) and selected area electron diffraction (SAED). The structures of the graphene and Al/graphene composite powder were examined using a Rigaku Ultima Type Ⅳ X-ray diffractometer equipped with a Cu $K\alpha$ radiation (λ = 0.154 056 nm) with 40 kV of the working voltage, 30 mA of the working current, 5°~80° of the scanning range and 0.01° of the step size. The Raman spectra of the samples were determined using an inVia Reflex-type microscopic confocal laser Raman spectrometer with incident laser light at a wavelength of 532 nm. The porous structure of the sample was characterized by an ASAP2020 automatic specific surface area and porosity analyzer, and the specific surface area of the sample was determined.

2 Results and discussion

2.1 Surface analysis

The graphene used in the experiment was a commercially available graphene, which was prepared by the redox method. Therefore, the oxygen-containing groups such as hydroxyl group, carbonyl group, and epoxy group were presented on the surface of the graphene.

Fig.1 presents the comparison of the FTIR spectra of graphene and Al/graphene composite powder. Characteristic peaks of graphene in the infrared spectrum were observed for the -OH stretching vibration absorption peak at 3 452 cm^{-1}, and the C-O stretching vibration absorption peak at 1 125 cm^{-1}. In addition, the absorption peaks at 1 648, 1 639 and 1 546 cm^{-1} were produced from the C=C stretching vibration of the sp^2 structure in graphene[20]. No absorption peak corresponding to C=O was observed

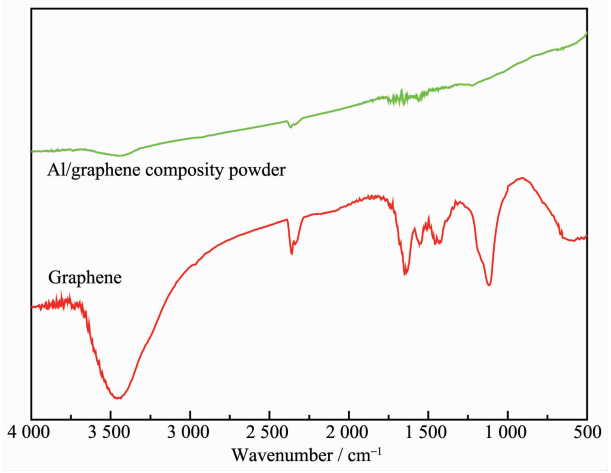

Fig.1 FTIR spectra of graphene and Al/graphene composite powder

in Fig.1, indicating that the graphene that had been used was not graphene oxide. For the Al/graphene composite powder, all the characteristic peaks of the graphene were weakened, especially the oxygen-containing groups because that the graphene was reduced by the reduction system and the surface and interlayers of the graphene were deposited with aluminum during electroless plating[21]. Therefore, FTIR spectroscopy provided convincing evidence that graphene was indeed reduced by the system to facilitate electroless plating.

Fig.2 (a,b) show the SEM images of Al/graphene composite powder. It can be seen that the graphene was spatially curved after electroless aluminum plating to form pores of different sizes and irregularities. The formation of these pores could be attributed to the action of aluminum. Because the graphene is multi-layered, the interlayer spacing was increased by ultrasound during the experiment. After the aluminum alkyl sesquihalide was reduced by NaH, the metal aluminum atoms were more likely to enter the interlayer voids, grow and extend, and interact with the defect regions in the graphene to generate a tensile force, which caused the graphene to bend and form ink-bottle-type pores. Fig.2(c,d) show the EDS spectra of spot 1 and spot 2 in Fig.2(a,b), respectively. The spot 1 was a point on the agglomerate of aluminum, which was very bright under electron microscopy. It can be seen from Fig.2(c) that the aluminum content was low, substantially existed in the form of alumina and contained a small amount of aluminum chloride, which indicated that the aluminum atom was staked and then oxidized. The spot 2 in Fig.2(b) was bright and the overall distribution was uniform. Fig.2 (d) shows that the aluminum content was high and only a very small amount of aluminum was oxidized; furthermore, most of them still existed in an elemental form, indicating that the coating of graphene could protect the aluminum element in the hole from being oxidized. There were a lot of spots the same as spot 2 after electroless plating. When Gr/Al is made of Al/graphene composite powder with aluminum or aluminum alloy, it can greatly improve the compatibility of graphene with metal and meet the requirements of the

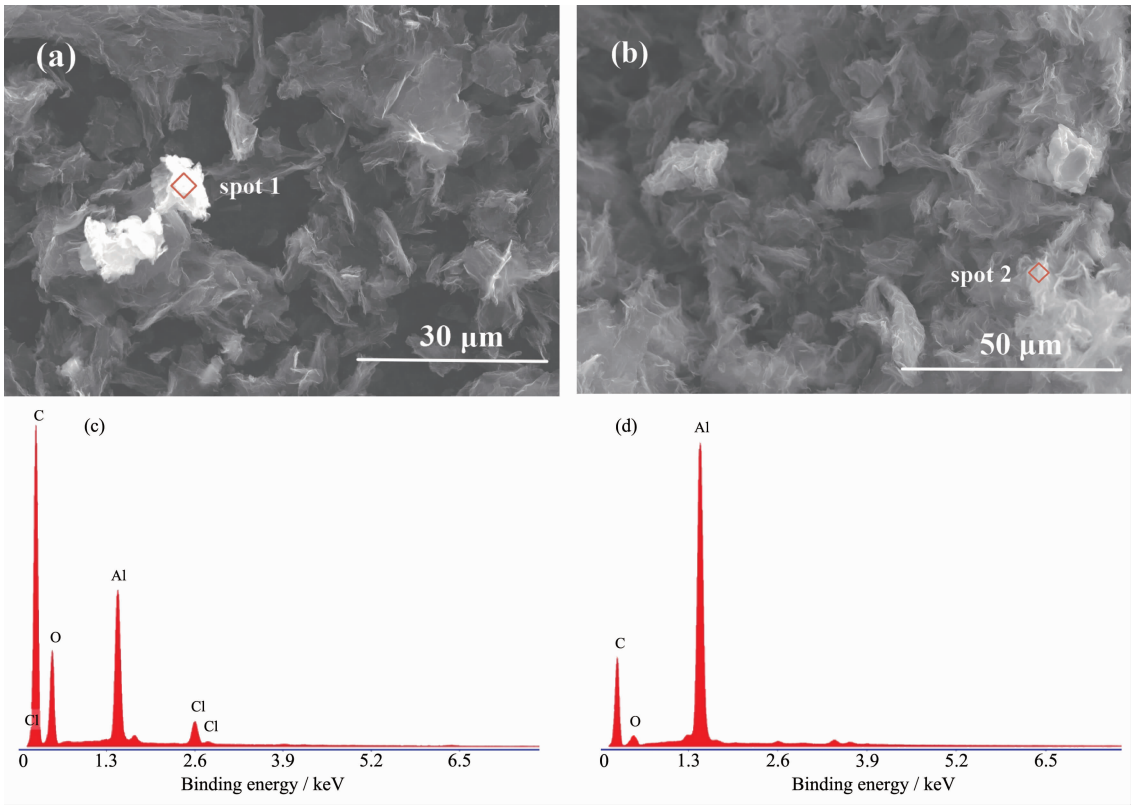

Fig.2 (a, b) SEM images of Al/graphene composite powder; (c) Composition analysis at spot 1; (d) Composition analysis at spot 2

SLM for material.

2.2 Structural analysis

As shown in Fig.3(a), according to the classification method proposed by the International Union of Pure and Applied Chemistry, the adsorption isotherm curve of the Al/graphene composite powder presented typical type Ⅳ adsorption behaviors at −196 ℃ and the H3-type hysteresis loop. The adsorption of N_2 molecules was single-layer and multi-layer adsorption in the micropores and mesopores, respectively, and the adsorption curve grew with a high slope in the relative pressure range of $0 < P/P_0 < 0.45$, which indicated the large number of micropores and mesopores. In addition, these pores provided enough space to adsorb N_2 molecules. At the relative pressure range of $0.45 < P/P_0 < 1$, the adsorption curve rised sharply, and unsaturation occured at the end of the curve. This situation indicated that a certain number of macropores were present in the sample, and the N_2 molecules caused capillary condensation in these pores, resulting in a significant increase in the amount of adsorption. Furthermore, as seen in Fig.3, there was a clear hysteresis loop, which proved the presence of open (parallel plate holes with four open sides) and the ink-bottle micro- and mesopores in the sample. The swelling of micropores and mesopores resulted in irreversible absorption of N_2 molecules in these pores. Besides, the irreversible chemical interactions between N_2 and the surface of the sample may also cause a hysteresis loop in the lower relative pressure range. Because of the presence of open (parallel plate holes with four open sides) and ink-bottle macro-pores and mesopores in the sample, the N_2 molecules showed capillary condensation, resulting in a significant hysteresis loop in the higher relative pressure range.

As shown in Fig.3(b), the pore size distribution curve shows that the mesopores and micropores accounted for the majority, and the maximum pore diameter was 1.6 ~3.7 nm. However, the curve was wide, and the pore diameter was not uniform. The Brunauer-Emmett-Teller specific surface area of the Al/graphene composite powder was 91 $m^2 \cdot g^{-1}$, which was much lower than the theoretical specific surface area of single-layer graphene. On the one hand, the graphene that has been used was multi-layered. On the other hand, graphene underwent spatial bending deformation to form a cladding structure after aluminum plating, so a large amount of surface area was not available for nitrogen adsorption. And this part of the surface area that could not be used for N_2 adsorption was combined with aluminum. So when Al/graphene composite powder is finally used for the preparation of Gr/Al, it can greatly improve the compatibility of graphene with the metal matrix.

Fig.4 presents the Raman spectra of graphene and Al/graphene composite powder. The raw graphene exhibited a D band and G band at 1 332 and 1 566 cm^{-1} in Fig.4(a), respectively, and the appearance of the D band indicated that the graphene was defective. The form of defects can be expressed as oxygen-containing groups, carbon-carbon double bonds,

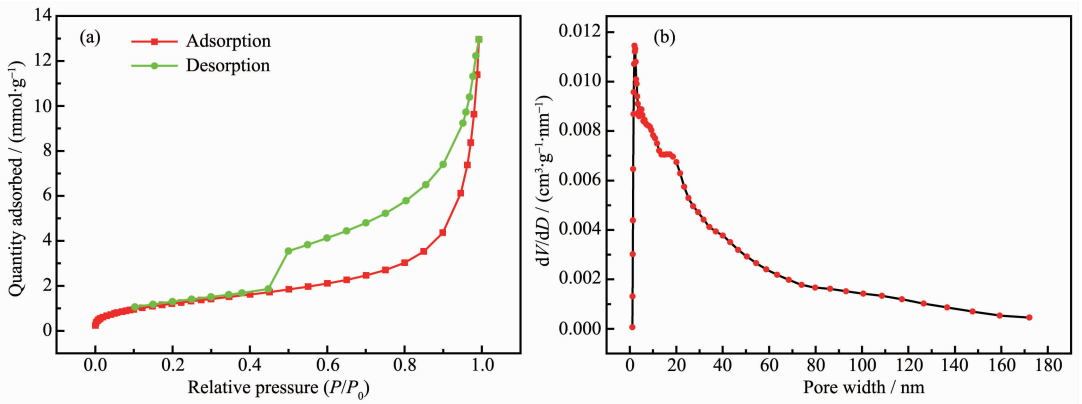

Fig.3　(a) N_2 adsorption-disorption isotherms of the Al/graphene composite powder;
(b) Pore size distribution curve from the desorption branch

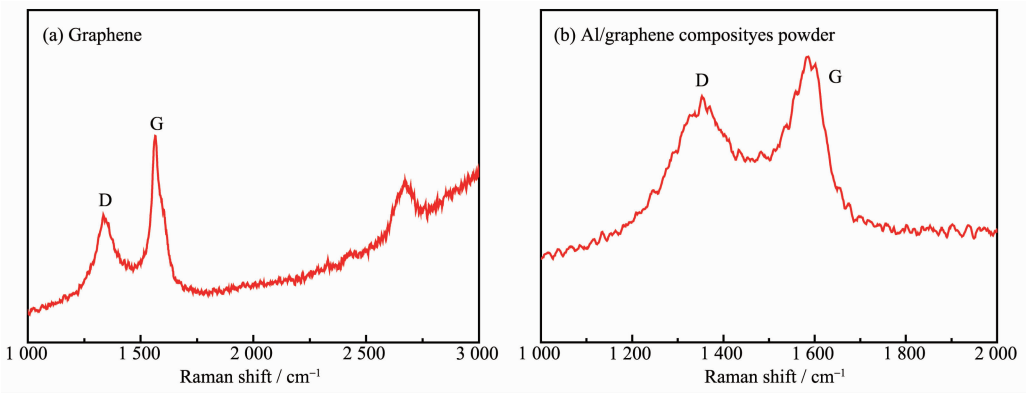

Fig.4 Raman spectra of graphene and Al/graphene composite powder

carbon five-membered rings, and carbon seven-membered rings, which indirectly verify the correctness of the infrared spectra of Fig.1. The position of the G band appeared at 1 566 cm^{-1}, which is lower than the literature[22] (1 580 cm^{-1}). The shape of the 2D band appearing at 2 677 cm^{-1} was asymmetrical, indicating that the graphene used was a multilayered structure because the G band had red-shift with the increase of the number of graphene layers. Fig.4 (b) shows that the peaks at 1 353 and 1 583 cm^{-1} belong to D band and G band of the Al/graphene composite powder, respectively. Obviously, the Al/graphene composite powder had a blue-shift relative to the raw material graphene, and the D band and G band positions were almost identical to the single-layer graphene. The reason is that it could cause the pitch of the graphene layer to increase when the aluminum atoms entered into the interlayer of the graphene, exhibiting some of the properties of the single-layer graphene.

It can be found that I_D/I_G (the intensity ratio of the D peak to the G peak) changed from 0.704 to 1.013, indicating that the degree and disorder of graphene defects were increased after electroless plating.

Fig.5 presents the XRD patterns of the graphene and Al/graphene composite powder. The very weak diffraction peak at 2θ=10.9° corresponded to the (002) plane of graphene oxide, and the weak diffraction peak of the graphite (100) plane was located at 2θ= 42.9°. Moreover, there was a broad but insufficiently strong diffraction peak at 2θ=24.0°, corresponding to the (002) plane of the expanded graphite; however, the 2θ angle of this diffraction peak was smaller than the theoretical value, and the interplanar spacing d= 0.368 4 nm was calculated from the Bragg′s law. In summary, the graphene with low crystallinity was obtained by a redox method for graphite, and the oxygen-containing groups existed on the surface.

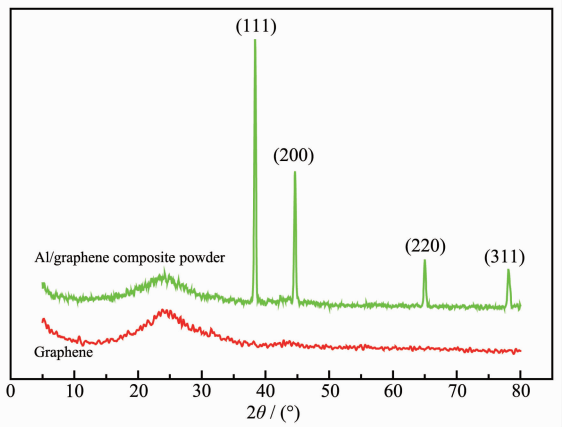

Fig.5 XRD patterns of graphene and Al/graphene composite powder

The characteristic peaks of Al were clearly discernible (PDF No.04-0787) in the XRD pattern of the Al/graphene composite powder. It can be seen from Fig.5 that there were four strong diffraction peaks for 2θ at 38.5°, 44.7°, 65.1° and 78.2°, corresponding to (111), (200), (220) and (311) plane, respectively. In addition, the diffraction peak of the (002) plane of the expanded graphite was located at 2θ= 24.0° and the weak diffraction peak of the graphite (100) plane was located at 2θ=42.3°. However, the diffraction peaks corresponding to Al_4C_3 were not detected. Briefly, the bonding between the graphene

after aluminum plating and the aluminum is not based on chemical bonds but physical interactions.

2.3 Microscopic surface analysis

To analyze the adsorption of aluminum on the surface and layers of graphene, the following model assumptions were made:

(1) The system is a constant temperature and pressure system that is not influenced by external factors;

(2) There are α-phase (graphene phase) and β-phase (metal aluminum phase), and the phase interface is SS, as shown in Fig.6;

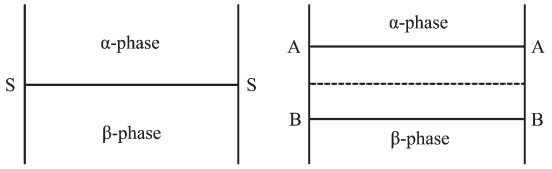

Fig.6　Schematic diagram of the surface phase

(3) The phase between the AA surface and the BB surface in Fig.6 is the surface phase (including by-products such as sodium bromide and alkane of the reactions in the solution). The properties at AA surface are the same as the α-phase and the properties at BB surface are identical with the β-phase. Thus, all changes that occur at the interface are included in the surface phase.

The volumes of the two phases from the bulk phases α and β to the SS face are represented by V_α and V_β, respectively. Assuming that the concentrations are uniform in V_α and V_β, the total amount of substance of component $\boldsymbol{i}$ in the whole system is $c_{i,\alpha}V_\alpha+c_{i,\beta}V_\beta$, $c_{i,\alpha}$ and $c_{i,\beta}$ are the concentrations of component $\boldsymbol{i}$ in the α-phase and β-phase, respectively. However, because the concentrations in the surface phase is not uniform, the value is different from the actual amount of substance (n_i), and the difference is represented by $n_{i,\sigma}$, then:

$$n_{i,\sigma}=n_i-(c_{i,\alpha}V_\alpha+c_{i,\beta}V_\beta) \tag{1}$$

This difference is the surface excess. The surface excess per unit area, or the surface excess of component $\boldsymbol{i}$ is:

$$\Gamma_i=\frac{n_{i,\sigma}}{A} \tag{2}$$

where A is the area of SS.

The two-component systems have the following formula:

$$G=n_1\mu_1+n_2\mu_2 \tag{3}$$

where G is the free energy; μ is a chemical potential.

For the surface phase, the surface energy σA also contributes to G_σ, so

$$G_\sigma=n_{1,\sigma}\mu_{1,\sigma}+n_{2,\sigma}\mu_{2,\sigma}+\sigma A \tag{4}$$

where G_σ is the free energy of the surface phase, σ is the surface tension, $\mu_{1,\sigma}$, $\mu_{2,\sigma}$ are the chemical potential of component **1** and **2** in the surface phase, respectively. Because the system is equilibrated at a certain temperature and pressure, the chemical potentials μ_1 and μ_2 of the respective components are constant in each phase and interface. Under constant temperature and pressure conditions, if an infinitesimal change occurs in the system, according to formula (**4**), then:

$$\mathrm{d}G_\sigma=n_{1,\sigma}\mathrm{d}\mu_{1,\sigma}+\mu_{1,\sigma}\mathrm{d}n_{1,\sigma}+n_{2,\sigma}\mathrm{d}\mu_{2,\sigma}+\mu_{2,\sigma}\mathrm{d}n_{2,\sigma}+\sigma\mathrm{d}A+A\,\mathrm{d}\sigma \tag{5}$$

If there is only a slight change in the interface area in the system under constant temperature and pressure, the amount of substance of component **1** and **2** on the interface changes, so that the surface excesses $n_{1,\sigma}$ and $n_{2,\sigma}$ also change accordingly. Minor changes in surface free energy should be:

$$\mathrm{d}G_\sigma=\mu_{1,\sigma}\mathrm{d}n_{1,\sigma}+\mu_{2,\sigma}\mathrm{d}n_{2,\sigma}+\sigma\mathrm{d}A \tag{6}$$

It can be derived from equations (**5**) and (**6**):

$$-A\,\mathrm{d}\sigma=n_{1,\sigma}\mathrm{d}\mu_{1,\sigma}+n_{2,\sigma}\mathrm{d}\mu_{2,\sigma} \tag{7}$$

Divide both ends by A and contact equation (**2**):

$$-\mathrm{d}\sigma=\Gamma_1\mathrm{d}\mu_{1,\sigma}+\Gamma_2\mathrm{d}\mu_{2,\sigma} \tag{8}$$

Assuming that the position of the surface is selected as being where the surface excess of the solvent (component **1**) is zero, which means $\Gamma_1=0$, then equation (**8**) can be re-written as follow:

$$-\mathrm{d}\sigma=\Gamma_2\mathrm{d}\mu_{2,\sigma} \tag{9}$$

At equilibrium, aluminum (component **2**) has the same chemical potential in the surface phase and the bulk phase, *ie*., $\mu_{2,\sigma}=\mu_2$ (in the bulk phase). In the bulk phase, $-\mathrm{d}\mu=RT\ln\alpha_2$, brought into equation (**9**),

$$\Gamma_2=-\frac{1}{RT}\left(\frac{\partial\sigma}{\partial\ln\alpha_2}\right)_T=-\frac{\alpha_2}{RT}\left(\frac{\partial\sigma}{\partial\ln\alpha_2}\right)_T \tag{10}$$

where Γ_2 is the surface excess of aluminum, α_2 is the activity of aluminum in solution, σ is the surface

tension of the solution, R is gas constant; T is thermodynamic temperature. The surface excess is much greater than the concentration of aluminum in the surface phase, at which point the surface excess can be approximated as the surface concentration. The concentration of aluminum (c) can be used instead of the activity α_2, so the subscript is omitted under constant temperature conditions, and the formula (*10*) can be written as:

$$\Gamma=-\frac{c}{RT}\frac{\mathrm{d}\sigma}{\mathrm{d}c} \quad (\mathbf{11})$$

where Γ is the adsorbing capacity, c is the concentration of solution. Because the aluminum obtained by the reduction is a solid and the concentration is constant (assuming **1**), the formula (**11**) can be simplified as:

$$\Gamma=-K\mathrm{d}\sigma \quad (\mathbf{12})$$

where K is a positive constant. That is, the surface excess of aluminum in the graphene surface and interlayer is related to the rate of change of solvent surface tension. If the surface tension becomes smaller ($\mathrm{d}\sigma<0$), the Γ is positive, which means that the concentration of aluminum in the surface layer is greater than in the solution, which is positive adsorption; if the surface tension becomes larger, the Γ is negative, which means the concentration of aluminum in the surface layer is less than in the solution, which is negative adsorption.

For the experimental system, the addition or not of NaH and the amount of addition have a great influence on the change of the surface tension of the solution. When NaH was absent from the system, the active alkyl aluminum sesquihalide decomposed at high temperature, and molecular bromine was formed. Then, the molecular bromine reacted with a trace amount of water in the system to form a mineral acid. The presence of this acid increased the surface tension of the solution. As shown in Fig.7(a), graphene

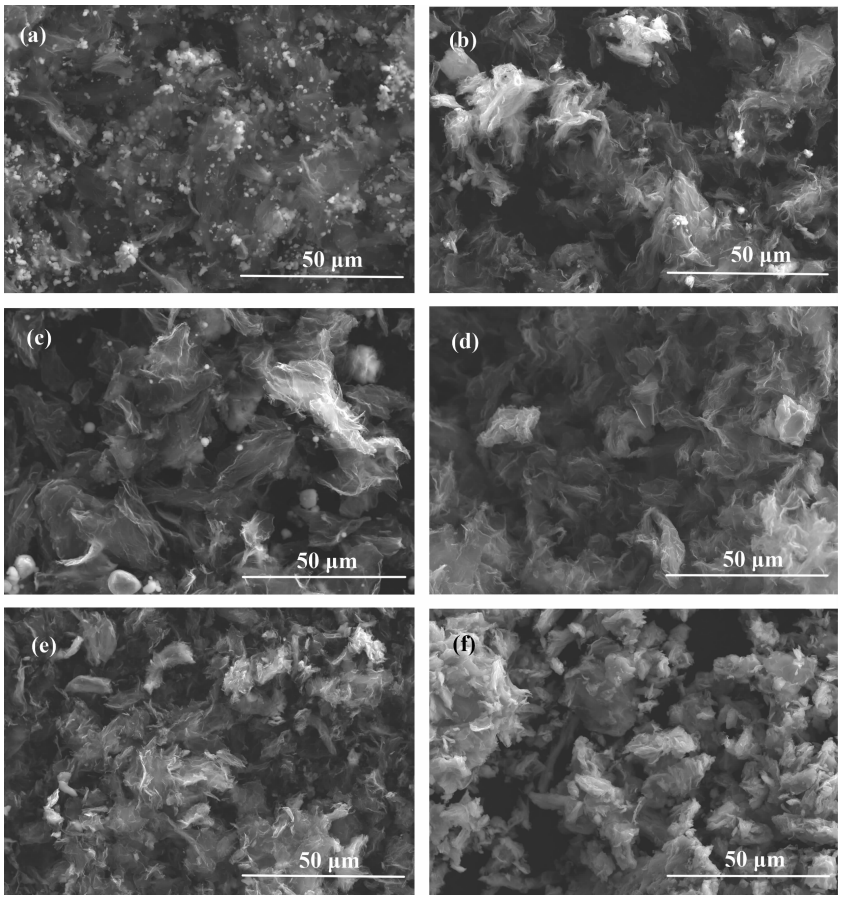

Added amount of NaH added from (a~f) were 0, 2, 4, 5, 6 and 8 g, respectively

Fig.7 SEM images of the Al/graphene composite powder corresponding to the added amount of NaH

exhibited negative adsorption on aluminum, that is, it did not adsorb aluminum, so aluminum itself agglomerated. With the addition of NaH, the alkyl aluminum sesquihalide was reduced and decomposed, and some by-products were changed from molecular bromine to inorganic salt sodium bromide, so that the amount of inorganic acid formed was reduced, and the change of surface tension of the solution was smaller than before. The degree of agglomeration of aluminum was weakened, and graphene begins to adsorb aluminum, as shown in Fig.7(b, c). When the added amount of NaH is slightly larger than the theoretical value, the reductive decomposition of the alkyl aluminum sesquihalide did not produce the by-product molecular bromine, which means the system did not contain a mineral acid. However, the presence of another by-product alkane reduced the surface tension of the solution, so that aluminum was adsorbed substantially on the surface and interlayers of the graphene without self-agglomeration, as shown in Fig.7(d). This situation is consistent with the ideal system assumption. As shown in Fig.7(e,f), with continuing to increase the amount of NaH, the extra NaH reduced the oxygen-containing groups of the graphene, so that the interlayer spacing becomes smaller, the force become larger, and the formed graphene/Al new phase was agglomerated.

3 Conclusions

Novel Al/graphene composite powder was prepared by a new organic phase electroless aluminum plating method in the current study. It is not necessary to perform any pretreatment (sensitization or activation) on graphene. At high temperature, the alkyl aluminum sesquihalide was decomposed and reduced to aluminum atoms by NaH, and the aluminum atoms adsorbed and deposited on the defects of the graphene. Ultrasound increased the spacing of the graphene layer, and the interaction of the aluminum atoms with the defect region caused the graphene sheet to be bent and formed a cladding structure. Microscopic surface analysis shows that the adsorption of aluminum by graphene is related to the rate of change of the surface tension of the solution. The situation that the surface tension of the solution become smaller that could facilitate the adsorption. The addition of NaH can not only reduce the activation energy of aluminum produced by the decomposition of the alkyl aluminum sesquihalide, but also indirectly reduce the surface tension of the solution. When the added amount of NaH was slightly larger than the theoretical value, the aluminum plating effect was the best, and no agglomeration occured. Consequently, the advantages of a relatively uniform distribution of Al on the surface and interlayers of graphene as well as special porous structure and high specific surface area may provide some information for solving the problems of the further preparation of Gr/Al, such as easy agglomeration of graphene in the aluminum matrix, and not being firmly bonded on the interface between the graphene and the matrix.

References:

[1] Li A, Zhang C, Zhang Y F, et al. *Polymers*, **2017**,**9**(9):437-454

[2] Nieto A, Bisht A, Lahiri D, et al. *Int. Mater. Rev.*, **2016**,**62**(5):241-302

[3] Soldano C, Mahmood A, Dujardin E. *Carbon*, **2010**,**48**(8):2127-2150

[4] Wang M, Duan X D, Xu Y X, et al. *ACS Nano*, **2016**,**10**(8):7231-7247

[5] Sun X M, Hao S, Li H P, et al. *Adv. Mater.*, **2013**,**25**(37):5153-5176

[6] Shen B, Li Y, Yi D, et al. *Carbon*, **2017**,**113**:55-62

[7] Porwal H, Grasso S, Reece M J. *Adv. Appl. Ceram.*, **2015**, **112**(8):443-454

[8] Miranzo P, Belmonte M, Osendi M I. *J. Eur. Ceram. Soc.*, **2017**,**37**(12):3649-3672

[9] Kumar H G P, Xavior M A. *Procedia Eng.*, **2014**,**97**:1033-1040

[10]Cho H, Rho H, Kim J H, et al. *ACS Appl. Mater. Interfaces*, **2017**,**9**(46):40801-40809

[11]Feng S W, Guo Q, Li Z, et al. *Acta Mater.*, **2017**,**125**:98-108

[12]Seretis G V, Kouzilos G, Polyzou A K, et al. *Nano Hybrids and Composites*, **2017**,**15**:26-35

[13]Zhao Z Y, Bai P K, Guan R G, et al. *Mater. Sci. Eng. A*,

2018,**734**:200-209

[14]Zhao Z Y, Guan R G, Zhang J H, et al. *Acta Metall. Sin.* (*Engl. Lett.*), **2017**,**30**:66-72

[15]Chen F, Gupta N, Behera R K, et al. *JOM*, **2018**,**70**(6):837-845

[16]Zhang H P, Xu C, Xiao W L, et al. *Mater. Sci. Eng. A*, **2016**,**658**:8-15

[17]Li J L, Xiong Y C, Wang X D, et al. *Mater. Sci. Eng. A*, **2015**,**626**:400-405

[18]Rashad M, Pan F, Yu Z, et al. *Prog. Nat. Sci.*: *Mater. Int.*, **2015**,**25**(5):460-470

[19]Zhang Z W, Liu Z Y, Xiao B L, et al. *Carbon*, **2018**,**135**:215-223

[20]LI Juan(李娟), ZHAO An-Ting(赵安婷), SHAO Jiao-Jing(邵姣婧), et al. *Chinese J. Inorg. Chem.*(无机化学学报), **2017**, **33**(7):1231-1235

[21]Muszynski R, Seger B, Kamat P V. *J. Phys. Chem. C*, **2008**, **112**(14):5263-5266

[22]Dresselhaus M S, Jorio A, Hofmann M, et al. *Nano Lett.*, **2010**,**10**(3):751-758